Journal of Computational Physics 228 (2009) 1056–1070

Contents lists available at ScienceDirect

Journal of Computational Physics

journal homepage: www.elsevier.com/locate/jcp

Comparison between lattice Boltzmann method and Navier–Stokes high order schemes for computational aeroacoustics

Simon Marié [a,b,*,1], Denis Ricot [b,2], Pierre Sagaut [a,3]

[a] Institut Jean le Rond d'Alembert, UMR CNRS 7190, 4 Place Jussieu case 162 Tour 55-65, 75252 Paris Cedex 05, France
[b] Renault Research Departement, TCR AVA 163, 1 avenue du golf, 78288 Guyancourt Cedex, France

ARTICLE INFO

Article history:
Received 20 September 2007
Received in revised form 25 September 2008
Accepted 12 October 2008
Available online 25 October 2008

Keywords:
Computational aeroacoustics
Lattice Boltzmann
Finite-differences
Runge–Kutta
Dispersion
Dissipation
Von Neumann analysis

ABSTRACT

Computational aeroacoustic (CAA) simulation requires accurate schemes to capture the dynamics of acoustic fluctuations, which are weak compared with aerodynamic ones. In this paper, two kinds of schemes are studied and compared: the classical approach based on high order schemes for Navier–Stokes-like equations and the lattice Boltzmann method. The reference macroscopic equations are the 3D isothermal and compressible Navier–Stokes equations. A Von Neumann analysis of these linearized equations is carried out to obtain exact plane wave solutions. Three physical modes are recovered and the corresponding theoretical dispersion relations are obtained. Then the same analysis is made on the space and time discretization of the Navier–Stokes equations with the classical high order schemes to quantify the influence of both space and time discretization on the exact solutions. Different orders of discretization are considered, with and without a uniform mean flow. Three different lattice Boltzmann models are then presented and studied with the Von Neumann analysis. The theoretical dispersion relations of these models are obtained and the error terms of the model are identified and studied. It is shown that the dispersion error in the lattice Boltzmann models is only due to the space and time discretization and that the continuous discrete velocity Boltzmann equation yield the same exact dispersion as the Navier–Stokes equations. Finally, dispersion and dissipation errors of the different kind of schemes are quantitatively compared. It is found that the lattice Boltzmann method is less dissipative than high order schemes and less dispersive than a second order scheme in space with a 3-step Runge–Kutta scheme in time. The number of floating point operations at a given error level associated with these two kinds of schemes are then compared.

1. Introduction

Computational aeroacoustic (CAA) has become an important subject since the advancement of powerful and efficient computers. The main purpose of CAA is to predict the near- and far-field noise radiated by immersed solid bodies or turbulent flows [8,29] via accurate and reliable simulations. Therefore, CAA solvers must be able to capture compressibility effects to correctly estimate the pressure fluctuations generated by the flow. They also must be accurate enough to propagate the

* Corresponding author. Address: Institut Jean le Rond d'Alembert, UMR CNRS 7190, 4 Place Jussieu case 162 Tour 55-65, 75252 Paris Cedex 05, France.
E-mail addresses: marie@lmm.jussieu.fr, simon@heclectics-pictures.com (S. Marié), denis.ricot@renault.com (D. Ricot), sagaut@lmm.jussieu.fr (P. Sagaut).
[1] Ph.D. Student, Université Paris 6 and Renault.
[2] Research engineer, Renault SAS.
[3] Professor, Université Paris 6, Paris.

0021-9991/$ - see front matter © 2008 Elsevier Inc. All rights reserved.
doi:10.1016/j.jcp.2008.10.021

information from the source region to the far-field. In this paper, we focus on the propagative capabilities of numerical schemes. Because in many practical cases the acoustic fluctuations are very weak compared with aerodynamic ones, propagation of acoustic waves in CAA necessitates high order accurate schemes. The spatial derivatives are classically approximated using high order finite-differences in space while time integration is performed thanks to a Runge–Kutta algorithm. Following the idea of Tam and Webb [30] dealing with optimizing the schemes by minimizing the dispersion and dissipation error, most of classical high order schemes have been revisited in the past few years [1,3]. Compact schemes were also studied [17] but we will focus on explicit schemes in this study.

Recently, the lattice Boltzmann method [6,21], has been studied for aeroacoustic purposes [4,7,24]. The main advantage of such a method is its ability to approximate the weakly compressible 3D Navier–Stokes equations with a simple algorithm, which is well suited for parallel computing. The lattice Boltzmann method is based on statistical mechanics and relies on microscopic quantities instead of macroscopic ones. It has been shown [7,20,21,24] that the lattice Boltzmann model is a second order scheme that could provide good qualitative results [4,24,31]. This must be pointed out because a second order scheme is theoretically unadapted for CAA requirements. In this paper, we aim at rigorously comparing the lattice Boltzmann method with the classical schemes in terms of aeroacoustic capabilities. Some accuracy analyses of the lattice Boltzmann method have been made using Taylor series expansion [18,23] and some qualitative comparisons with other CFD methods have been performed [10,11]. For aeroacoustic and wave propagation purposes, the Von Neumann analysis is more convenient and has been used for stability analysis [28]. Let's note that this well known tool has been recently revisited and extended [27]. The idea is here to apply this analysis to the classical high order schemes and to the lattice Boltzmann method in order to quantify the aeroacoustic capabilities of each scheme. This analysis consists of looking for plane wave solutions of the linearized equations. In the limit of linear acoustics, this analysis is very efficient to recover the dispersion and dissipation relation. Indeed, plane wave solutions yield the relation between the wavenumber $\mathbf{k}$ and the wave pulsation ω. Each scheme has its own dispersion and dissipation relations which will be used as a reference for their comparison.

In the first section, the linearized Navier–Stokes equations are presented and their exact plane wave solutions are computed. The principal characteristics of the classical high order schemes are then discussed and their Von Neumann analysis is described. Here, we point out that effects of both space and time discretization are taken into account at the same time. Then we present the lattice Boltzmann models and the associated key parameters. Three different models are presented: the discrete velocities Boltzmann equation (DVBE) without any space and time discretization, the classical lattice Boltzmann model (LBM–BGK) and the multiple relaxation time model (LBM–MRT). The Von Neumann analysis of these models is performed considering the linearized lattice Boltzmann equations. Results and comparisons are presented in the last section. The dispersion and dissipation relations of the different model are displayed and the errors committed by the different schemes are discussed.

2. Compressible linearized Navier–Stokes equations in 3D

2.1. Exact plane wave solutions

In this section, we look for plane wave solutions of the 3D linearized Navier–Stokes equations to get the theoretical dispersion and dissipation relations for a plane wave propagating in a perfect gas. The obtained solutions will be used as references for the dispersion and dissipation analysis of the different schemes. First, the linearization of all the quantities U is done around the mean flow as $U = U_0 + U'$ assuming that U' has a small amplitude and that U_0 is uniform in order to suppress gradient effects. Moreover, we will consider an isothermal flow to be consistent with the lattice Boltzmann theory. This hypothesis will be further explained in the next section and restricts the analysis to weakly compressible fluids where the Mach number is still small enough ($Mach < 0.4$). Then, the energy equation will be linearized considering the internal energy. This equation can be written in the isothermal configuration as

$$\frac{\partial \rho e}{\partial t} + \frac{\partial \rho e u_i}{\partial x_i} = -p\frac{\partial u_i}{\partial x_i} + \tau_{ij}\frac{\partial u_i}{\partial x_j} \tag{1}$$

where τ_{ij} the local stress tensor. It is to be noticed that the last term in the right-hand side of Eq. (1) is a 2nd order term and will not appear in the linearized equation. The perfect gas internal energy $\rho e = \frac{p}{\gamma - 1}$ will be used to complete the equations. Under these hypotheses, the 3D linearized Navier–Stokes equations can be written in the following conservative form:

$$\frac{\partial \mathbf{U}'}{\partial t} + \frac{\partial}{\partial x_1}[\mathbf{E}'_\mathbf{e} - E'_\mathbf{v}] + \frac{\partial}{\partial x_2}[\mathbf{F}'_\mathbf{e} - F'_\mathbf{v}] + \frac{\partial}{\partial x_3}[\mathbf{G}'_\mathbf{e} - G'_\mathbf{v}] = 0 \tag{2}$$

where $\mathbf{U}'$ is the unknown vector, $bfE'_\mathbf{e}, \mathbf{F}'_\mathbf{e}, \mathbf{G}'_\mathbf{e}$ the Eulerian flux and $\mathbf{E}'_\mathbf{v}, \mathbf{F}'_\mathbf{v}, \mathbf{G}'_\mathbf{v}$ the viscous flux given by

$$\mathbf{U}' = \begin{pmatrix} \rho' \\ \rho_0 u' \\ \rho_0 v' \\ \rho_0 w' \\ p' \end{pmatrix} \mathbf{E}'_\mathbf{e} = \begin{pmatrix} \rho' u_0 + \rho_0 u' \\ p' + u_0 \rho_0 u' \\ u_0 \rho_0 v' \\ u_0 \rho_0 w' \\ u_0 p' + \gamma p_0 u' \end{pmatrix} \mathbf{F}'_\mathbf{e} = \begin{pmatrix} \rho' v_0 + \rho_0 v' \\ v_0 \rho_0 u' \\ p' + v_0 \rho_0 v' \\ v_0 \rho_0 w' \\ v_0 p' + \gamma p_0 v' \end{pmatrix} \mathbf{G}'_\mathbf{e} = \begin{pmatrix} \rho' w_0 + \rho_0 w' \\ w_0 \rho_0 u' \\ w_0 \rho_0 v' \\ p' + w_0 \rho_0 w' \\ w_0 p' + \gamma p_0 w' \end{pmatrix}$$

$$\mathbf{E}'_{\mathbf{v}} = \begin{pmatrix} 0 \\ \tau'_{11} \\ \tau'_{12} \\ \tau'_{13} \\ 0 \end{pmatrix} \mathbf{F}'_{\mathbf{v}} = \begin{pmatrix} 0 \\ \tau'_{21} \\ \tau'_{22} \\ \tau'_{23} \\ 0 \end{pmatrix} \mathbf{G}'_{\mathbf{v}} = \begin{pmatrix} 0 \\ \tau'_{31} \\ \tau'_{32} \\ \tau'_{33} \\ 0 \end{pmatrix}$$

where τ' is the linearized stress tensor. We will see in the following that a non-zero bulk viscosity coefficient has to be taken into account. The linearized stress tensor will be written in its general form

$$\tau'_{ij} = \rho_0 \nu \left(\frac{\partial u'_i}{\partial x_j} + \frac{\partial u'_j}{\partial x_i} - \frac{2}{3} \frac{\partial u'_k}{\partial x_k} \delta_{ij} \right) + \rho_0 \xi \frac{\partial u'_k}{\partial x_k} \delta_{ij} \tag{3}$$

where $\rho_0 \xi = \eta$ corresponds to the bulk viscosity coefficient. Eq. (2) being a linear equation, it can be written in a matricial form

$$\frac{\partial \mathbf{U}'}{\partial t} + \mathbf{M}_{\mathbf{E}} \frac{\partial \mathbf{U}'}{\partial x_1} + \mathbf{M}_{\mathbf{F}} \frac{\partial \mathbf{U}'}{\partial x_2} + \mathbf{M}_{\mathbf{G}} \frac{\partial \mathbf{U}'}{\partial x_3} = 0 \tag{4}$$

where $\mathbf{M}_{\mathbf{E}}, \mathbf{M}_{\mathbf{F}}$ and $\mathbf{M}_{\mathbf{G}}$ are matrices given in the Appendix. We can now look for plane wave solutions of Eq. (4) which suggests that vector $\mathbf{U}'$ has the following form:

$$\mathbf{U}' = \begin{pmatrix} \hat{\rho}' \\ \rho_0 \hat{u}' \\ \rho_0 \hat{v}' \\ \rho_0 \hat{w}' \\ \hat{p}' \end{pmatrix} exp[i(\mathbf{k}.\mathbf{x} - \omega t)] \tag{5}$$

assuming that $\hat{\rho}', \hat{u}', \hat{v}', \hat{w}'$ and $\hat{p}'$ are complex values. Injecting Eq. (5) in Eq. (4) induces a simplification in the derivative terms ($\partial/\partial x_j \rightarrow ik_j$ and $\partial/\partial t \rightarrow -i\omega$) which leads to the general eigenvalue problem:

$$\omega \mathbf{U}' = \mathbf{M}^{\mathrm{NS}} \mathbf{U}' \tag{6}$$

with $\mathbf{M}^{\mathrm{NS}} = k_x \mathbf{M}_{\mathbf{E}} + k_y \mathbf{M}_{\mathbf{F}} + k_z \mathbf{M}_{\mathbf{G}}$. Then, analytical solutions of this equation are found to be:

$$\begin{cases} \omega_1 &= \mathbf{k} \cdot \mathbf{u}_0 - i|\mathbf{k}|^2 \mathscr{N} + |\mathbf{k}| c_0 \left[1 - \left(\frac{|\mathbf{k}| \mathscr{N}}{c_0} \right)^2 \right]^{1/2} \\ \omega_2 &= \mathbf{k} \cdot \mathbf{u}_0 - i|\mathbf{k}|^2 \mathscr{N} - |\mathbf{k}| c_0 \left[1 - \left(\frac{|\mathbf{k}| \mathscr{N}}{c_0} \right)^2 \right]^{1/2} \\ \omega_3 &= \mathbf{k} \cdot \mathbf{u}_0 - i \mid \mathbf{k}|^2 \nu \\ \omega_4 &= \omega_3 \\ \omega_5 &= \mathbf{k} \cdot \mathbf{u}_0 \end{cases} \tag{7}$$

with $\mathscr{N} = \frac{2}{3}\nu + \frac{1}{2}\xi$ and $\mathbf{u}_0 = [u_0, v_0, w_0]$. These five modes correspond to the following three different physical modes introduced by Chu and Kovasznay [15] to analyze weak compressible turbulent fluctuations (see [26] for an exhaustive description):

(1) ω_1 and ω_2 (in the following $\omega_\pm$) denotes the acoustics mode propagating with velocity $c_\pm = |\mathbf{u}_0| cos(\widehat{\mathbf{k}\mathbf{u}_0}) \pm c_0[1 - (\frac{|\mathbf{k}|\mathscr{N}}{c_0})^2]^{1/2}$ and dissipation rate of $-\mathscr{N}|\mathbf{k}|^2$.
(2) $\omega_3 = \omega_4 = \omega_T$ corresponds to the shear mode (or vorticity mode) that propagates at speed $c_T = |\mathbf{u}_0| cos(\widehat{\mathbf{k}\mathbf{u}_0})$ and dissipation rate $-\nu|\mathbf{k}|^2$.
(3) ω_5 corresponds to the entropy mode. Because of the isothermal hypothesis, this mode corresponds to a none-dissipative wave propagating with the shear mode.

For our study, the transport coefficients will be set to their classical values in air: $c_0 = 340$ m/s and $\nu = 1.510^{-5}$ m^2/s. It should be noticed that the non-dimensional number $\mathscr{S} = \frac{|\mathbf{k}|\mathscr{N}}{c_0}$ can be written in the form $\mathscr{S} = \frac{|\tilde{\mathbf{k}}|\mathscr{N}}{c_0 \Delta x}$ with $\tilde{\mathbf{k}} = \frac{2\pi}{N_{ppw}}$ where N_{ppw} is the number of grid points per wavelength. For the maximum value of $\tilde{\mathbf{k}} = \pi$ which correspond to two points per wavelength and for the case of a zero bulk viscosity coefficient: $\mathscr{N} = \frac{2}{3}\nu$, $\mathscr{S}^2$ is still very small ($log(\mathscr{S}^2) = -2log(\Delta x) - 14$) for the considered values of Δx. Therefore, it will be neglected in the following.

The solutions (7) describe the behavior of a linear propagative phenomenon predicted by the 3D isothermal Navier–Stokes equations. We will use these modes as a reference in the following to study the effect of different space and time discretization on these solutions.

2.2. Space and time discretization

Numerical simulation needs to evaluate the derivative terms with a discrete operator. In CAA, the computation of the acoustic field is classically performed using high order schemes in both space and time. These schemes have been actively studied in the past few years. In this work, we will consider the explicit schemes [30], but implicit schemes can also be used for acoustic propagation [17]. The most classical approach is to use finite-differences for space and Runge–Kutta algorithms for time.

2.2.1. Space discretization

A general approximation of the spatial derivatives by a centered $2N+1$ point stencil finite-difference scheme for a given quantity $\mathbf{U}$ can be written as

$$\frac{\partial \mathbf{U}}{\partial x_i}(x_i^0) = D_{x_i}(x_i^0) = \frac{1}{\Delta x_i}\sum_{j=-N}^{N} a_j \mathbf{U}(x_i^0 + j\Delta x_i) \tag{8}$$

where a_j are the coefficients related to a given finite-difference scheme. The standard coefficients are computed to match the Taylor series expansion of the spatial derivatives up to a certain order of accuracy. Other families of coefficients are computed to minimize the dispersion error. Such schemes are called DRP for "dispersion relation preserving". The first DRP schemes were developed by Tam and Webb in [30] and were followed by other families of schemes using different error criteria. In the following, the optimized 6th order Bogey scheme [3] will be used. We want to highlight here that the theoretical order of such a scheme, in terms of taylor series, is not strictly equal to six. Indeed, the coefficients of the scheme are optimized for dispersion and does not match those of the taylor series expansion. Thus, the order is slightly less than six. However, for convenient reasons, we will refer to this scheme as a 6th order one in the following. Moreover, it should be noticed that centered finite-differences are not dissipative and may yield numerical instabilities. For this reason, they are often supplemented by spatial filters to damp the instabilities. In this paper, we will not take these filters into account.

2.2.2. Time discretization

The time integration is classically done with Runge–Kutta algorithms for a differential equation of the form:

$$\frac{\partial \mathbf{U}}{\partial t} = F(\mathbf{U}) \tag{9}$$

A p-stage Runge–Kutta algorithm can be expressed, if F is a linear function, by the following form:

$$\mathbf{U}^{n+1} = \mathbf{U}^n + \sum_{j=1}^{p} \gamma_j \Delta t^j F^j(\mathbf{U}^n) \tag{10}$$

where F^j denotes the multiple composition of function F such as: $F^2(\mathbf{U}) = F(F(\mathbf{U}))$. The coefficients γ_j are chosen to match the Taylor series of the time derivative in their classical form, or to minimize the dispersion and dissipation errors [1].

2.2.3. High order schemes dispersion and dissipation relation

In the classical approach, dispersion and dissipation are studied separately for space discretization and time integration. Space discretization yields a relation between the exact wavenumber $k\Delta x$ and the simulated one $k^*\Delta x$ whereas time integration gives a relation between the exact pulsation $\omega\Delta t$ and the simulated one $\omega^*\Delta t$. For our study, we propose to get the dispersion and dissipation relations for the full discretization. This approach is necessary for the comparison with lattice Boltzmann schemes in which the space and time discretizations cannot be distinguished (see Section 3). In order to achieve these relations for the 3D linearized Navier–Stokes equation, we have to look for plane wave solutions of Eq. (4) discretized in space and time. Applying the same analysis as in 2.1 and writing Eq. (4) in the form (9) we get the following system:

$$\begin{cases} e^{-i\omega}\mathbf{U^n} &= \mathbf{U^n} + \sum_{j=1}^{p} \gamma_j \Delta t^j F^j(\mathbf{U}^n) \\ F(\mathbf{U}^n) &= -\mathbf{M_E}\mathbf{U^n}\frac{1}{\Delta x_1}\sum_{j=-N}^{N} a_j e^{ijk_1\Delta x_1} - \mathbf{M_F}\mathbf{U^n}\frac{1}{\Delta x_2}\sum_{j=-N}^{N} a_j e^{ijk_2}\Delta x_2 \\ &\quad -\mathbf{M_G}\mathbf{U^n}\frac{1}{\Delta x_3}\sum_{j=-N}^{N} a_j e^{ijk_3\Delta x_3} \end{cases} \tag{11}$$

Considering a uniform mesh with $\Delta x_1 = \Delta x_2 = \Delta x_3 = \Delta x$, and expressing function F as $F(\mathbf{U^n}) = (c_0/\Delta x)\mathbf{\Lambda}\mathbf{U^n}$ where $\mathbf{\Lambda}$ is a matrix given in Appendix, Eq. (11) thus leads to the general eigenvalue problem:

$$e^{-i\omega}\mathbf{U^n} = [\mathbf{I} + \sum_{j=1}^{p} \gamma_j (CFL)^j \mathbf{\Lambda}^j]\mathbf{U^n} = \mathbf{M}_d^{\mathrm{NS}}\mathbf{U^n} \tag{12}$$

where $\mathbf{I}$ is the identity matrix and the CFL number is defined by $\mathrm{CFL} = c_0 \frac{\Delta t}{\Delta x}$. It should be noticed that the coefficient Δx is taken from the expression of the derivative approximation to make the CFL number appearing in the expression. Therefore, Δx appears in the expressions of matrices $\mathbf{M_E}, \mathbf{M_F}$ and $\mathbf{M_G}$. For the computations, the coefficient Δx will be taken equal to one without loss of generality. Indeed, because the CFL number is set to a constant value, Δx is an arbitrary parameter. The dispersion relation of the discretized linearized Navier–Stokes equations is obtained with the solutions of Eq. (12). The bulk viscosity is taken equal to zero so that $\mathscr{N}$ becomes $\mathscr{N} = \frac{2}{3}\nu$. In such a case the reference solutions (7) becomes:

$$\begin{cases} \omega_{\pm} &= |\mathbf{k}|(|\mathbf{u}_0| cos(\widehat{\mathbf{k}\mathbf{u}_0}) \pm c_0) - \frac{2}{3} i |\mathbf{k}|^2 \nu \\ \omega_{\mathbf{T}} &= |\mathbf{k}||\mathbf{u}_0| cos(\widehat{\mathbf{k}\mathbf{u}_0}) - i|\mathbf{k}|^2 \nu \end{cases} \tag{13}$$

The solutions of Eq. (12) depend on both space and time discretizations. Table 1 summarizes the different tested cases, indicating the order of the finite-difference discretization and the number of steps for the Runge–Kutta algorithm. The letter "o" denotes optimized DRP schemes. The last three columns refer to the symbol used to plot the solutions for the different modes.

Fig. 1 compares the solutions of cases 1, 2 and 3 with the exact solutions (7) obtained in Section 2.1. In classical approaches, the curves always represent the evolution of $\mathbf{k}^*$ as a function of $\mathbf{k}$ for the space discretization and ω^* as a function of ω for the time discretization. In our study, because the influence of space and time discretization are taken into account in the same time, we chose to represent directly the evolution of ω^* versus $\mathbf{k}$. For each case, the acoustic modes are clearly more dissipated than the shear mode. The CFL number for these results has been taken to 0.57 to match the lattice Boltzmann CFL (see Section 3). This value refers to the CFL number computed with the sound speed: $\mathrm{CFL}^{ac} = c_0 \frac{\Delta t}{\Delta x}$ and induces a CFL number relative to the mean flow: $\mathrm{CFL}^{shear} = M_a \mathrm{CFL}^{ac}$ where M_a is the Mach number $M_a = U_0/c_0$. For the configurations without mean flow, the CFL^{shear} vanishes. In a general way, and for subsonic flow, we have $\mathrm{CFL}^{shear} < \mathrm{CFL}^{ac}$. This explains that the acoustic modes are always more dissipated than the shear mode.

3. Boltzmann models

In this section, the idea is not to explain the lattice Boltzmann theory in details but to expose the main ideas and the hypothesis useful for our study. Then we will develop the procedure to derive the theoretical dispersion of the lattice Boltzmann schemes.

3.1. Continuous Boltzmann equation

The continuous Boltzmann Eq. (14) comes from statistical mechanics and hold on statistical quantities instead of macroscopic quantities:

$$\frac{\partial f}{\partial t} + c \frac{\partial f}{\partial x_i} = \left(\frac{\partial f}{\partial t}\right)_{coll} \tag{14}$$

$$\left(\frac{\partial f}{\partial t}\right)_{coll} = -\frac{1}{\tau}[f - f^{eq}] \tag{15}$$

where $f(\mathbf{x}, \mathbf{c}, t)$ is the single-particle distribution function and $\mathbf{c}$ the microscopic particle velocity. A Chapman–Enskog procedure [5] of the continuous Boltzmann equation with the BGK [2] collision operator (15) can recover the compressible Navier–Stokes equations using the definition of momentums:

$$\rho = \int_{\mathscr{R}^3} f dc \tag{16}$$

$$\rho \mathbf{u} = \int_{\mathscr{R}^3} \mathbf{c} f dc \tag{17}$$

Table 1
Definitions of tested cases. The "Space" column indicates the finite-differences schemes order. The 6th order corresponds to the Bogey scheme [3]. The "Time" column indicates the number of steps for the Runge–Kutta algorithm. The 6-step optimized Runge–Kutta has been proposed by Berland et al. [1]. The last three columns indicate the symbols used to plot Figs. 1, 8 and 9.

Case	Space	Time	Mach	Ac +	Ac −	Shear
1a	2nd Order	3-step	0.0	△	▽	□
1b			0.2			
2a	Tam and Webb o	3-step	0.0	+	×	○
2b			0.2			
3a	6th Order o	6-step o	0.0	☆	✡	◇
3b			0.2			

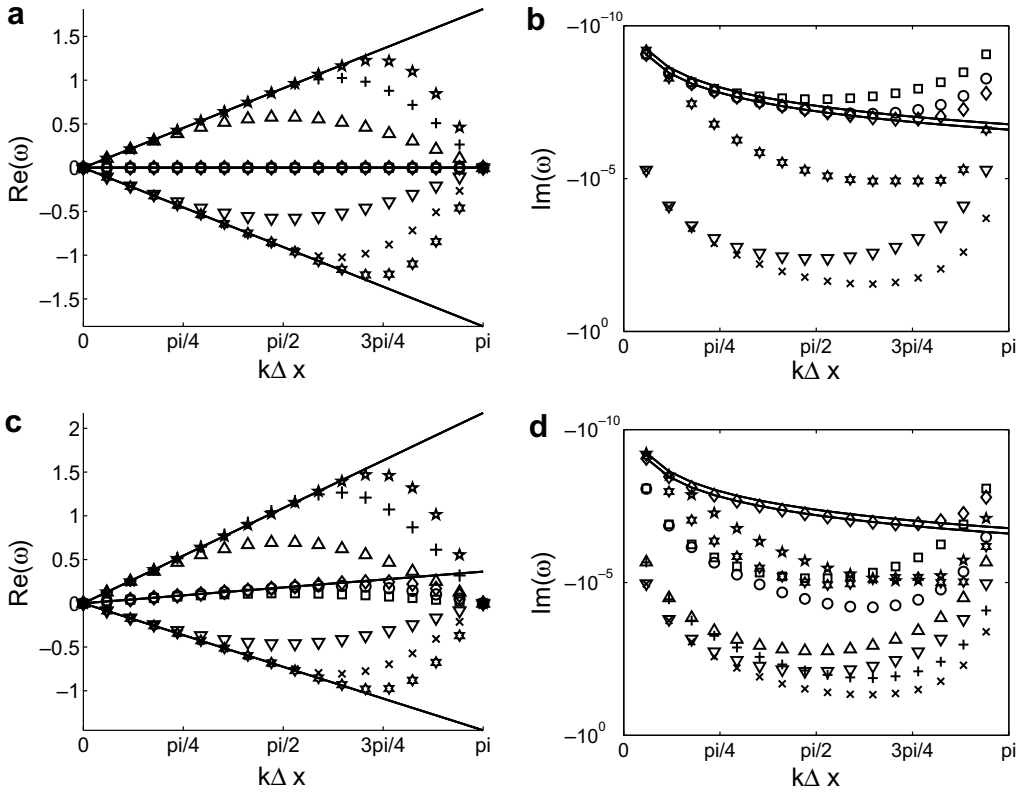

Fig. 1. Real and imaginary part evolution of ω for the linearized Navier–Stokes equations: — Exact solutions. (a and b): $M_a = 0.0$, (c and d) $M_a = 0.2$. Captions given in Table 1.

3.2. Discrete velocity Boltzmann equation

He and Luo [13] have shown that the continuous Boltzmann–BGK equation could be solved for some discrete points of the velocity space representing the lattice if the equality between continuous and discrete momentums were satisfied. Then, Eq. (14) yields the discrete velocity Boltzmann equation (DVBE):

$$\frac{\partial f_\alpha}{\partial t} + c_{\alpha,i}\frac{\partial f_\alpha}{\partial x_i} = -\frac{1}{\tau}\left[f_\alpha - f_\alpha^{eq}\right] \tag{18}$$

The discrete velocity models are computed with a Gauss–Hermite quadrature approximation of the equilibrium distribution function. This procedure [13] allows for the computations of isothermal models only. In this case, the development of the third order momentum implies the bulk viscosity coefficient to become [9]: $\xi = 2/3\nu$. The most popular velocity-model involves 19 discrete velocities in 3D (D3Q19). This model will be used in our study. However, it can be shown [22] that the restriction to 19 discrete velocities modifies the strain rate tensor, leading to

$$\tau_{ij} = \rho\nu\left(\frac{\partial u_i}{\partial x_j} + \frac{\partial u_j}{\partial x_i}\right) - \tau\frac{\partial \rho u_i u_j u_k}{\partial x_k} \tag{19}$$

The cubic term $O(M_a^3)$ restricts lattice Boltzmann simulations to small Mach numbers. To fully describes the D3Q19 velocity model, the equilibrium state must be defined through the equilibrium distribution function derived from the Hermite polynomial expansion of the Maxwell–Boltzmann equilibrium truncated to the second order:

$$f_\alpha^{eq}(\mathbf{x},t) = \rho\omega_\alpha\left(1 + \frac{\mathbf{u}.\mathbf{c}_\alpha}{\tilde{c}_0^2} + \frac{(\mathbf{u}.\mathbf{c}_\alpha)^2}{2\tilde{c}_0^4} - \frac{|\mathbf{u}|^2}{2\tilde{c}_0^2}\right) \tag{20}$$

where $\tilde{c}_0 = \frac{1}{\sqrt{3}}$ is the adimensional sound speed and ω_α the weighting factors. The macroscopic quantities ρ and $\mathbf{u}$ can be expressed with the discrete momentums:

$$\rho = \sum_\alpha f_\alpha \tag{21}$$

$$\rho\mathbf{u} = \sum_\alpha \mathbf{c}_\alpha f_\alpha \tag{22}$$

and the viscosity coefficient is given by

$$\tilde{\nu} = \tilde{c}_0^2 \tilde{\tau} \tag{23}$$

As in Sections 2.1 and 2.2.3, we want to look for plane wave solution of Eq. (18). The approach is the same but the linearization will be done on the distribution functions, considering a uniform mean part f_α^0 and a fluctuating part f'_α such as

$$f'_\alpha = A_\alpha exp[i(\mathbf{k}.\mathbf{x} - \omega t)] \tag{24}$$

The non-linear terms of the Boltzmann equations are contained in the equilibrium distribution function (Eq. 20). By using a Taylor expansion of this function, we can write:

$$f^{eq}(f_\alpha^{(0)} + f'_\alpha) = f_\alpha^{eq,(0)} + \frac{\partial f_\alpha^{eq}}{\partial f_\beta}|_{f_\beta = f_\beta^{(0)}} \cdot f'_\alpha + o(f'^2_\alpha) \tag{25}$$

The difficulty is to evaluate the derivation of the compressible equilibrium distribution function. The exact expression is found using the mathematical software Maple. Applying this analysis to Eq. (18), we get the linear equation:

$$i\omega \mathbf{f}' = M^{\mathrm{DVBE}} \mathbf{f}' \tag{26}$$

with $\mathbf{f}'$ the vector of the fluctuating part of the distribution functions and M^{DVBE} is a matrix defined in the Appendix. In 2D, Luo [16] evaluated the eigenvalues using successive approximations in $\mathbf{k}$. In our case, we use a linear algebra library (LAPACK) to solve the eigenvalue problem on the 19×19 matrix M^{DVBE}. This eigenvalue problem gives a relation between ω and the eigenvalues of the matrix M^{DVBE}. These values depend on three parameters which are, the relaxation time τ, the propagation direction held by vector $\mathbf{k}[k_x, k_y, k_z]$ and the mean flow $\mathbf{u_0}[u_0, v_0, w_0]$. Thus, by this result, we get the dispersion and dissipation relation with $Re(\omega)$ and $Im(\omega)$. The bulk viscosity for the Boltzmann scheme is taken to $\xi = \frac{2}{3}\nu$ so that $\mathscr{N} = \nu$. The reference solutions (7) thus become:

$$\begin{cases} \omega_\pm &= |\mathbf{k}|(|\mathbf{u}_0| cos(\widehat{\mathbf{k}\mathbf{u}_0}) \pm c_0) - i|\mathbf{k}|^2 \nu \\ \omega_\mathbf{T} &= |\mathbf{k}||\mathbf{u}_0| cos(\widehat{\mathbf{k}\mathbf{u}_0}) - i|\mathbf{k}|^2 \nu \end{cases} \tag{27}$$

Fig. 2 displays the evolution of the different modes for the discrete velocity Boltzmann model with, $\mathbf{k} = [k_x, 0, 0]$, $\tilde{\tau} = 0.0025$ and $\mathbf{u_0} = [0, 0, 0.2c_0]$. Here, the relaxation time has been chosen to match the value of the shear relaxation time given in [10] for the MRT model. This choice will be justified in the following for the comparison between MRT and BGK model. The three physical modes predicted by the theory and described by Eq. (27) are recovered in the Boltzmann results of Fig. 2. The DVBE curves match perfectly the exact dispersion.

However, eventhough DVBE predicts the exact dissipation without mean flow ($M_a = 0.0$), an error appears in the DVBE dissipation for a non-zero mean flow. This error is the direct effect of the $O(M_a^3)$ non-physical term of Eq. (19). This can be verified by adding this term in the Navier–Stokes analysis of Section 2.1. In this case, the matrices $\mathbf{M_E}$, $\mathbf{M_F}$ and $\mathbf{M_G}$ are modified and the solutions (7) of the eigenvalue problem (6) take the form:

$$\begin{cases} \omega_\pm &= \mathbf{k}\cdot\mathbf{u}_0 - i|\mathbf{k}|^2[\mathscr{N} - \frac{3}{2}\tau\mathbf{u}_0^2] \pm |\mathbf{k}|c_0\sqrt{1 + \mathscr{P}(M_a)} \\ \omega_\mathbf{T} &= \mathbf{k}\cdot\mathbf{u}_0 - i\,|\,\mathbf{k}|^2[\nu - \tau\mathbf{u}_0^2] \end{cases} \tag{28}$$

where $\mathscr{P}(M_a) = 3\tau\mathscr{N}|\mathbf{k}|^2 M_a^2 - \frac{3}{4}[\tau|\mathbf{k}|c_0]^2 M_a^4 + i\tau|\mathbf{k}|c_0 M_a^3$. The solutions (27) are recovered if the mean flow is set to zero. Fig. 3 shows the ratio between the numerical dissipation and the theoretical dissipation obtained with solutions (27) and (28).

We can note that the dissipation error does not depends on $\mathbf{k}$ and is the direct ratio between the imaginary parts of solutions (28) and (27). This ratio can be written as follows:

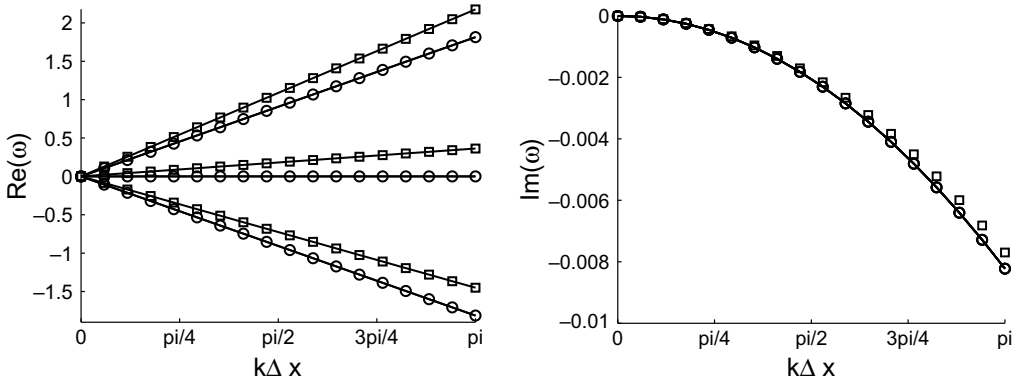

Fig. 2. Evolution of the DVBE dispersion: (a) and dissipation (b) –: Exact solutions ○: DVBE for $M_a = 0.0$ and □) for $M_a = 0.2$.

$$\begin{cases} r_T &= 1-\frac{\tilde{\tau}\tilde{U}_0^2}{\tilde{\nu}} = 1-M_a^2 \\ r_\pm &= 1-\frac{3\tilde{\tau}\tilde{U}_0^2}{2\tilde{\nu}} \pm \varepsilon = 1-\frac{3}{2}M_a^2 \pm \varepsilon \end{cases} \tag{29}$$

where $\varepsilon = \frac{c_0}{\nu}\Im\left(\sqrt{\frac{1+\mathscr{P}(M_a)}{\mathbf{k}^2}}\right)$. If we focus on the circles of Fig. 3, we note that the dissipation error disappears with solutions (28). This means that expression (28) represents the exact analytical dispersion relation of the discrete velocity Boltzmann equation.

Here, we have shown that the velocity discretization had no influence on the dispersion and that the dissipation error was linked to the error term added in the strain rate tensor (19). We can now focus on the influence of space and time discretization by studying the lattice Boltzmann models.

3.3. The lattice Boltzmann models

3.3.1. The LBM–BGK model

Historically, the lattice Boltzmann model has been developed from lattice gas models [6,21]. Here we present the "*a priori*" construction of the model introduced recently [13]. The so-called lattice Boltzmann equation can be obtained by integrating Eq. (18) along the c_α characteristic:

$$f_\alpha(\mathbf{x}+c_\alpha\Delta t, t+\Delta t) - f_\alpha(\mathbf{x},t) = -\frac{1}{\tau}\int_0^{\Delta t}[f_\alpha(\mathbf{x}+c_\alpha s, t+s) - f_\alpha^{eq}(\mathbf{x}+c_\alpha s, t+s)]ds \tag{30}$$

By evaluating the integral with the trapezoidal method and with the variable change [9]:

$$g_\alpha(\mathbf{x},t) = f_\alpha(\mathbf{x},t) + \frac{\Delta t}{2\tau}(f_\alpha(\mathbf{x},t) - f_\alpha^{eq}(\mathbf{x},t)) \tag{31}$$

we obtain the lattice Boltzmann equation on g_α:

$$g_\alpha(\mathbf{x}+c_\alpha\Delta t, t+\Delta t) = g_\alpha(\mathbf{x},t) - \frac{\Delta t}{\tau_g}[g_\alpha(\mathbf{x},t) - g_\alpha^{eq}(\mathbf{x},t)] + O(\Delta t^3) \tag{32}$$

with $\tau_g = \tau + \frac{1}{2}$ and $g_\alpha^{eq} = f_\alpha^{eq}$. It should be noticed that the construction of Eq. (32) enforces the space and time discretization to be linked by the relation:

$$\Delta t = \frac{\tilde{c}_0\Delta x}{c_0} \tag{33}$$

This link between space and time discretization is an important feature of the lattice Boltzmann method and enforces the CFL number ($c_0\Delta t/\Delta x$) to be the same for each simulations ($\mathrm{CFL} = \tilde{c}_0$).

3.3.2. The LBM–MRT model

The multiple relaxation time model [10,16], has been presented recently and is an alternative to the standard BGK model. The idea is not to present this model in details but to summarize the main features which are relevant for our purposes. The MRT model uses a different relaxation time for each momentum. The number of momentums must be equal to the number of discrete velocities. This constraint introduces a correspondence matrix P between the distribution function vector and the momentum one. The collision step of the algorithm must be carried out in the momentum space, whereas the propagation

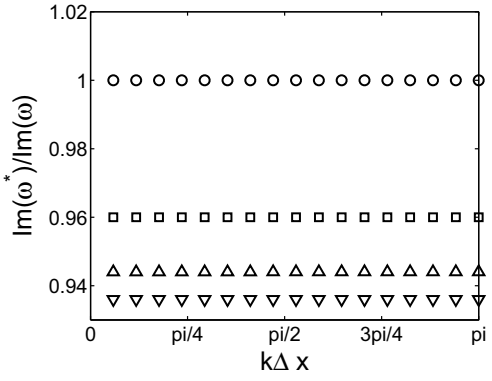

Fig. 3. Evolution of the DVBE dissipation error: □), △ and ▽ denote respectively the shear, acoustic (+) and acoustic (−) errors from exact solutions (27) and ○ denotes the errors for the three modes from exact solutions (28).

step is done in the physical space. The relaxation time in the collision term of Eq. (18) is then replaced by a diagonal matrix S containing the different relaxation times. This model allows us to control independently the relaxation of the different moments. The equation of such a model can be written as

$$\mathbf{g}(\mathbf{x}+\mathbf{c},t+1)=\mathbf{g}(\mathbf{x},t)-P^{-1}S[\mathbf{m}(\mathbf{x},t)-\mathbf{m_{eq}}(\mathbf{x},t)] \tag{34}$$

where $\mathbf{m}$ is the momentum vector such as $\mathbf{m}=P\mathbf{g}$ and S defined as follow:

$$S=diag[0,s_1,s_2,0,s_4,0,s_4,0,s_4,s_9,s_{10},s_9,s_{10},s_{13},s_{13},s_{13},s_{16},s_{16}] \tag{35}$$

where $s_i=1/\tau_i$. In the following, the relaxation times will be taken from [10]: $\tau_1=0.6098,\tau_2=0.6494,\tau_4=0.5264,\tau_9=\tau_{10}=\tau_{13}=\tau_{16}=0.5025$. Moreover, in classical MRT model the equilibrium distribution function is quite different than its Eq. (20) form and is similar to an incompressible model [14]. From this, the classical MRT model evaluates vector $\mathbf{m}^{eq}$ with:

$$\mathbf{m}^{eq}=P\mathbf{f}^{eq} \tag{36}$$

In this work, we will study the acoustic behavior of the MRT model with an equilibrium distribution function defined by Eq. (20). The viscosity coefficients are defined as follow:

$$\begin{cases} \nu &= \frac{1}{3}\left(\tau_9-\frac{1}{2}\right) \\ \xi &= \frac{2}{9}\left(\tau_1-\frac{1}{2}\right) \end{cases} \tag{37}$$

3.3.3. Theoretical dispersion and dissipation relations of the lattice Boltzmann models

To get the dispersion relation of the lattice Boltzmann models, the analysis is based on Eqs. (32) and (34). The linearization is made on the g_α quantities and the linear equilibrium is the same than in Section 3.2. Then we get the linear equation for the LBM–BGK model (38) and for the LBM–MRT model (39):

$$e^{-i\omega}\mathbf{g}'=M^{\mathrm{BGK}}\mathbf{g}' \tag{38}$$

$$e^{-i\omega}\mathbf{g}'=M^{\mathrm{MRT}}\mathbf{g}' \tag{39}$$

These new eigenvalue problems are solved to get the dispersion and dissipation relations. Figs. 4 and 5 compare the dispersion and dissipation evolution of the Lattice Boltzmann models to the theoretical ones which take the form:

$$\begin{cases} \omega_\pm &= |\mathbf{k}|[|\mathbf{u}_0|cos(\widehat{\mathbf{ku}_0})\pm c_0]-i|\mathbf{k}|^2\mathscr{N} \\ \omega_{\mathbf{T}} &= |\mathbf{k}||\mathbf{u}_0|cos(\widehat{\mathbf{ku}_0})-i|\mathbf{k}|^2\nu \end{cases} \tag{40}$$

where $\mathscr{N}=\nu$ for the LBM–BGK model and $\mathscr{N}=\frac{2}{3}\nu+\frac{1}{9}(\tau_1-\frac{1}{2})$ for the LBM–MRT model.

We remarks that LBM suffers from dispersion errors for the three physical modes. The dispersion error increases as the number of point per wavelength (related to the adimensional wavenumber) decreases. Comparing these results with these of DVBE, we can say that the dispersion introduced by the lattice Boltzmann models is only due to the space and time discretization. This means that the velocity discretization does not influence the plane wave dispersion. Moreover, it should be noticed that MRT and BGK models have exactly the same dispersion error. Fig. 5 shows the evolution of the dissipation for the lattice Boltzmann models with the previous parameters.

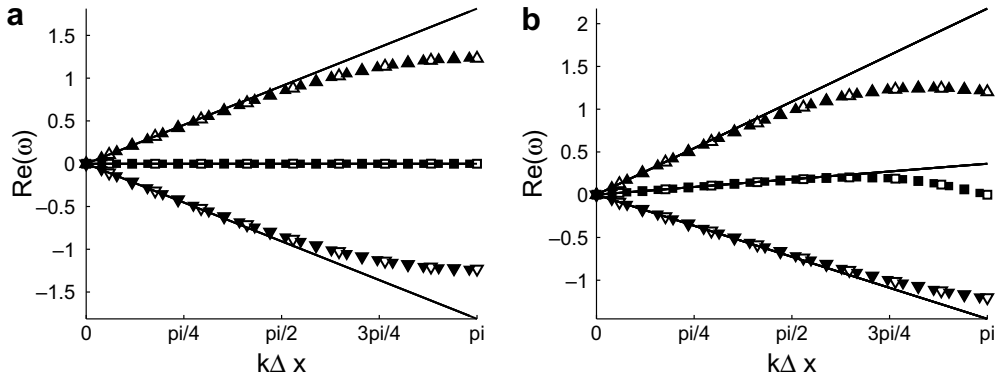

Fig. 4. Evolution of the dispersion ($Re[\omega]$) for the two lattice Boltzmann models with (a) $M_a=0.0$ and (b) $M_a=0.2$. –: Exact, $\triangle,\triangledown,\square$: Acoustic +, acoustic − and shear mode for LBM–BGK, ▲, ▼, ■: Acoustic +, acoustic − and shear mode for LBM–MRT.

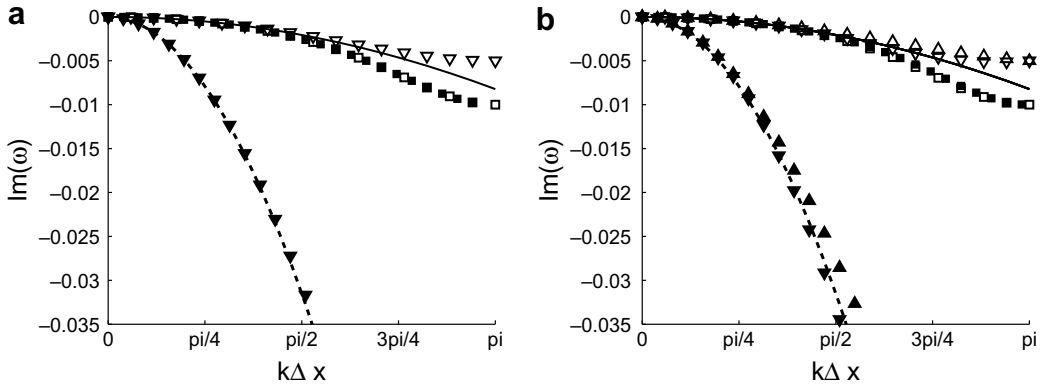

Fig. 5. Evolution of the dissipation ($Im[\omega]$) for the two lattice Boltzmann models with (a) $M_a = 0.0$ and (b) $M_a = 0.2$. – : Exact, △, ▽, □: Acoustic +, acoustic − and shear mode for LBM–BGK, ▲, ▼, ■: Acoustic +, acoustic − and shear mode for LBM–MRT.

In the MRT model, the bulk viscosity can be controlled independently with a different relaxation time. In a classical way, LBM–MRT models are built with a high value of the bulk viscosity to ensure a better stability. Indeed we observe a higher dissipation of the acoustic modes for the LBM–MRT model (Fig. 5) whereas the dissipation of the shear mode remains the same for LBM–MRT and LBM–BGK. As in the dispersion relation, it should be noticed that the dissipation error level is introduced by the space and time discretization.

Here, a rigorous comparison has been performed between BGK and MRT model. We have pointed out that the MRT model was not adapted for acoustic simulations, because of the high value of bulk viscosity, introducing higher acoustic dissipation. In the following, we will consider only the LBM–BGK model for the comparison with Navier–Stokes high order schemes.

3.3.4. Numerical simulations

We have performed numerical simulations to test the LBM accuracy and its dispersion and dissipation. For the computation we used the L-BEAM code based on the D3Q19 LBM–BGK model and coded with double precision [19]. In all the simulations, we use a uniform cubic grid of 80^3 meshes with periodical boundary conditions. The viscosity is set to $v = 1.510^{-5}$ m^2/s and $\Delta x = 1.25$ cm, which induces a relaxation time $\tau_g = 0.5000061$. To test the accuracy, we simulate a 3D pressure pulse and estimate the L_2 norm:

$$L_2 = \frac{1}{N}\sum_{i=1}^{N}\left(p_i^{th} - p_i^{num}\right)^2 \tag{41}$$

where N is the number of points along the pulse and p_ith represents the analytical solution given in [12] by

$$p'(x,y,z,t) = \frac{\varepsilon}{2\alpha\sqrt{\pi\alpha}}\int_0^{\infty}\xi^2 exp\left[-\frac{\xi^2}{4\alpha}\right]cos(c_0 t\xi)J_0(\xi\eta)d\xi \tag{42}$$

with $\varepsilon = 10^{-3}, \alpha = \ln 2/b_p^2, \eta = \sqrt{(x-U_0t)^2+y^2+z^2}$ and J_0 is the spherical Bessel function of first kind and order 0. The b_p parameter represents the resolution of the pulse (i.e $\sqrt{b_p}\Delta x$ meshes along the pulse length). In order to minimize the bound-

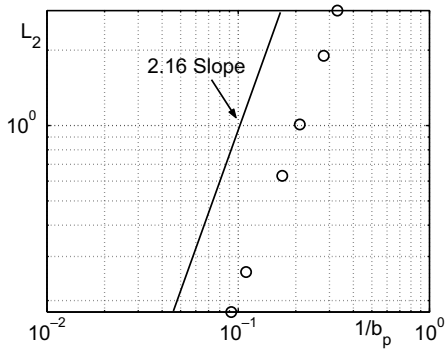

Fig. 6. L_2 norm evolution with the spatial resolution.

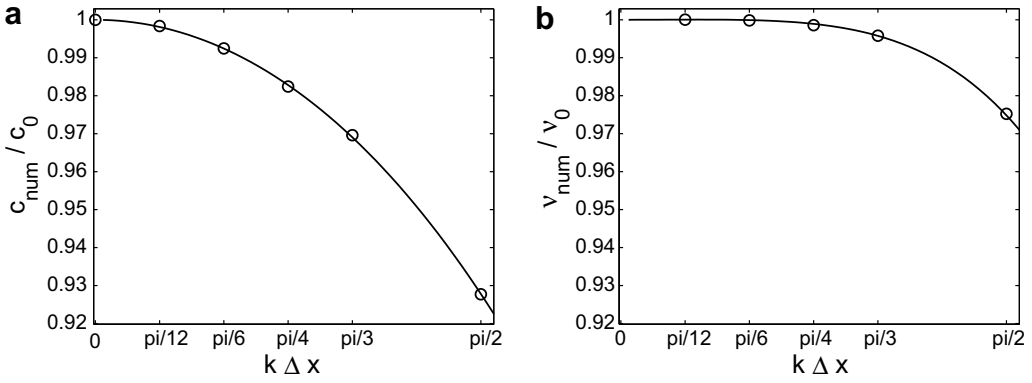

Fig. 7. Evolution of the ratio between numerical and theoretical values, with the adimensional wavenumber for $M_a = 0.0$. (a) Sound phase speed (dispersion), and (b) viscosity (dissipation). (—): theory, (○): simulations.

ary influence, the simulation is stopped when the pulse reaches the limit of the computational domain. The error norm is computed for different values of b_p. The evolution is plotted on Fig. 6.

The curve has a slope of 2.16 which corresponds to the numerical accuracy of LBM. This observed result is in good agreement with the theoretical 2nd order of the LBM.

Then, we have simulated a propagating acoustic wave in a periodical domain without mean flow to verify the dispersion and dissipation highlighted in the previous section. The computational domain corresponds to one wavelength in the propagating direction with five meshes in the other directions ($5 \times 5 \times N_{ppw}$ meshes). The boundary conditions are periodic and the acoustic wave travels along the *x-direction*. To have significant effects of dispersion and dissipation, we use 50,000 time-steps for the simulations. Here, we estimate the numerical sound speed variation with the resolution (numerical dispersion) and the viscosity variation (numerical dissipation). Fig. 7 compares these evolutions with the theoretical dispersion and dissipation relations presented on Figs. 4a and 5a. The theoretical evolution of sound speed is obtained by $\Re[\omega^*]/k$ and the viscosity by $-\Im[\omega^*]/k^2$.

The numerical simulations match perfectly the theoretical curves and validate the approach used to study the dispersion and dissipation relations. We can note here that for four points per wavelength ($k\Delta X = \pi/2$), the sound speed is correct to 93% and the viscosity to 97.5%.

4. Comparisons

We can now compare the dispersion and dissipation errors of the LBM–BGK scheme and the Navier–Stokes high-order schemes. In order to compare it rigorously, we have to find a good comparison criteria. This criteria will be the error committed on $Re(\omega^*)$ and $Im(\omega^*)$, function of the wavenumber. It can be written in the form:

$$\begin{cases} Err^{\Re}(\mathbf{k}) &= |\Re[\omega^*(\mathbf{k})\Delta t] - \Re[\omega^{th}(\mathbf{k})\Delta t]| \\ Err^{\Im}(\mathbf{k}) &= |\Im[\omega^*(\mathbf{k})\Delta t] - \Im[\omega^{th}(\mathbf{k})\Delta t]| \end{cases} \tag{43}$$

where * refers to the solutions of Eqs. (12), (38) and (39), and th refers to the exact solutions (13) and (40). These criteria will be computed for the same CFL number. The lattice Boltzmann models allow only one value of the CFL number given by $\mathrm{CFL}^{\mathrm{LBM}} = 1/\sqrt{3}$ which corresponds to the non-dimensional sound speed $\tilde{c}_0$. This value will be chosen for the Navier–Stokes schemes. Moreover the viscosity coefficient has to be carefully chosen to match the real simulated viscosity in lattice Boltzmann scheme and in classical scheme. In lattice Boltzmann simulations, the adimensional viscosity is given by $\tilde{\nu} = \tilde{c_0}^2\tilde{\tau}$ and in classical schemes by $\tilde{\nu} = \nu\frac{\Delta t}{\Delta x^2}$. This enforces the relaxation time to be $\tilde{\tau} = \frac{\nu CFL}{\Delta x \tilde{c_0}^2 c_0} = \frac{\nu\sqrt{3}}{c_0\Delta x}$ for the comparison.

Figs. 8 and 9 compare dispersion and dissipation errors in lattice Boltzmann schemes and Navier–Stokes cases 1, 2 and 3. First, we can note that the LBM dispersion is between a global second order scheme and an optimized third order in space with a 3-step Runge–Kutta in time. Although lattice Boltzmann method is a 2nd order accurate method, it has better dispersion capabilities than the classical 2nd order Navier–Stokes schemes. However, these results depend on the considered mode. For example, the LBM shear mode dispersion is very close to the optimized third order of Tam and Webb (Fig. 9). Then, we can note that for $k\Delta X \geqslant 3\pi/4$ (i.e under 2.6 points per wavelength), LBM has a dispersion error below all the Navier–Stokes schemes. This is due to centered finite-differences scheme which is not resolved for two points per wavelength ($\Re[\omega(k\Delta X = \pi)] = 0$). In a general way, we note a dissymmetry in the dispersion and the dissipation for a non-zero mean flow: the acoustic mode (+) is generally more dispersed than the acoustic mode (−) whereas this one is more dissipated than the (+) one. Moreover, dissipation results are clearly in the lattice Boltzmann favor. Even if the shear mode exhibits higher dissipation than the optimized 6th order Navier–Stokes schemes, the acoustic modes are clearly less dissipated with LBM. The large dissipation of the high order schemes is introduced by the Runge–Kutta algorithm.

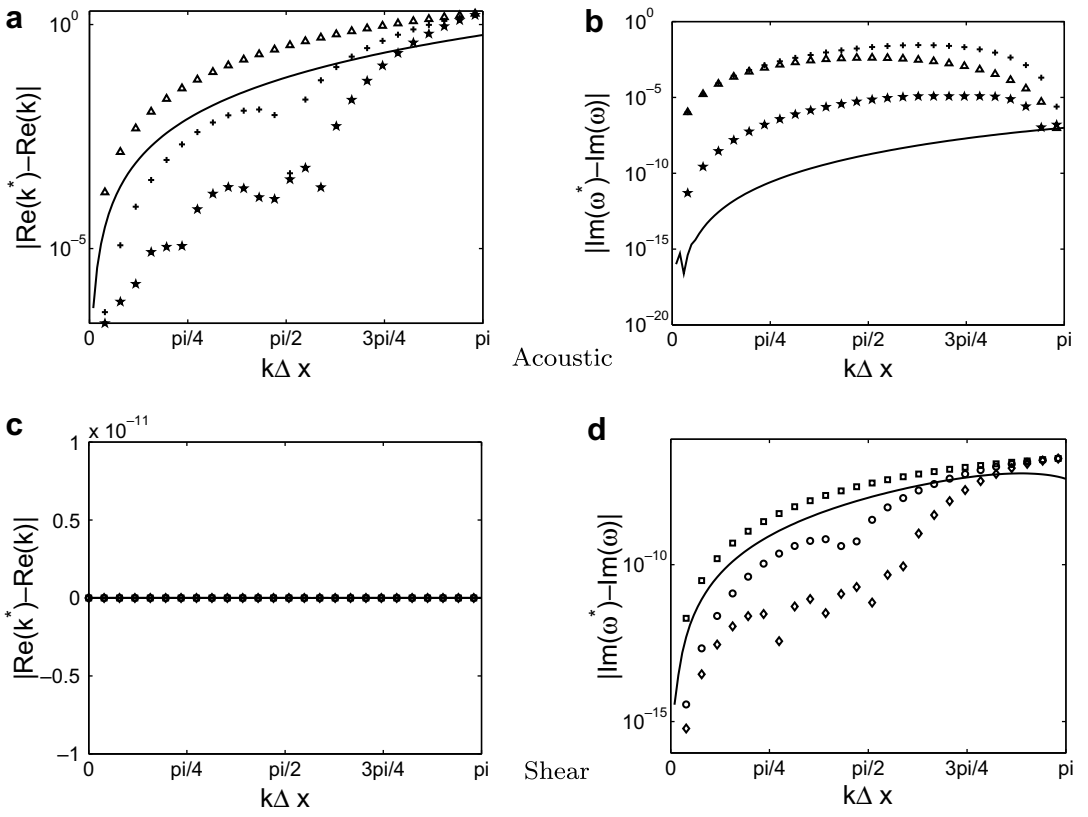

Fig. 8. (a–c) Dispersion, and (b–d) dissipation error with $M_a = 0.0$. (—) LBM, ($\triangle$, $\square$) 2nd order FD, ($+$, $\circ$) 3rd order optimized FD, ($\star$, $\Diamond$) 6th order optimized FD, See Table 1 for more informations.

So, we have shown that for iso-CFL and a same adimensional viscosity, LBM had better dispersion and dissipation capabilities than a 2nd order Navier–Stokes schemes. Now, to fully compare both discretization methods, the number of operations must be taken into account. Indeed, as presented previously, the lattice Boltzmann algorithm is very simple compared to the high order algorithms. We will focus here on the dispersion error for the acoustic mode+with a mean flow, which is the most unfavourable case for the LBM scheme. The number of operation N_{op} for each scheme must be computed for the same physical time T and depends on the CFL number and on the number of points per wavelength N_{ppw}:

$$N_{op} = \frac{Tc_0}{\Delta x}\frac{N_1 N_{ppw}}{\mathrm{CFL}} \tag{44}$$

where N_1 is the number of operation done during one iteration. A rigorous method to compare the speed of each scheme, consists in evaluating the number of operations necessary to achieve a given tolerated dispersion error. This number depends on the ratio between N_{ppw} and the CFL number. For the lattice Boltzmann scheme, because the CFL number could not be changed, the ratio is determined by the number of points per wavelength (Table 2).

For the classical schemes, the CFL number could be freely chosen and the minimum ratio $r = N_{ppw}/\mathrm{CFL}$ should be taken to minimize the number of operation (44). It appears that the minimum ratio is obtained for the greatest CFL. However, this one is limited by the stability condition. For example, it has been shown [30] that for CFL values greater than 1, the DRP schemes could become unstable because of the explicit centered spatial discretization. Indeed, the CFL number is the direct ratio between the physical propagation speed c_0 and the phase speed of the scheme $u_\phi = \Delta x/\Delta t$. For explicit schemes, a CFL > 1 implies $c_0 > u_\phi$ and the acoustic information cannot be propagated correctly. Consequently, for our study, we will consider CFL $= 1$ as a maximum value. (Table 2) sums up the informations relative to the minimum ratio r for each cases. Finally, we can compute the real ratio $R = \frac{N_{op}^{\mathrm{LBM}}}{N_{op}^{\mathrm{NS}}}$ between the number of operation made by the LBM and the classical schemes to reach a given tolerated dispersion error Table 3.

A ratio $R < 1$ means that the LBM is less expensive that the classical scheme and is found for all the tested cases excepted for case 2 with a tolerated error of 0.01% which corresponds to a ratio of 1.62. However, this ratio decreases fastly with CFL and reach the value of 0.99 for a *CFL* of 0.98. Thanks to these results, we can say that for a dispersion error greater or equal to 0.01%, the lattice Boltzmann scheme needs less FLOP than the classical finite-differences schemes. This shows that the lattice

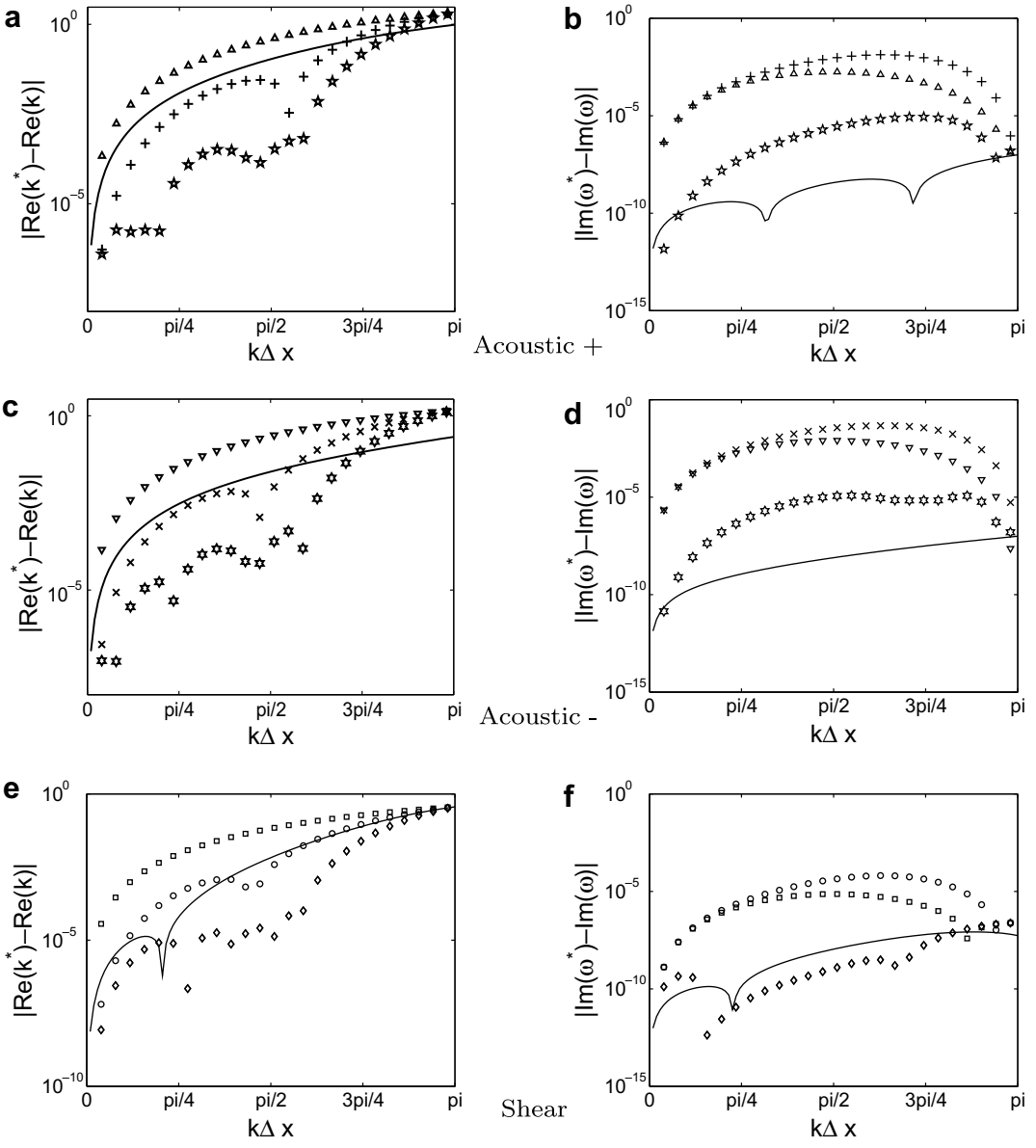

Fig. 9. (a)(c)(e) Dispersion, and (b)(d)(f) dissipation error with $M_a = 0.2$. (—) LBM, ($\triangle, \triangledown, \square$) 2nd order Navier–Stokes, ($+, \times, \circ$) 3rd order optimized Navier–Stokes, ($\star$, ✡, $\diamond$) 6th order optimized Navier–Stokes. See Table 1 for more informations.

Table 2
Smallest ratio $r = N_{ppw}/CFL$ for a dispersion error of 1%, 0.1% and 0.01%.

	NS Case 1	NS Case 2	NS Case 3	LBM
N_1	711	2862	11295	588
CFL	1.0	1.0	1.0	0.57
$r_{1\%}$	16.70	4.94	3.97	12.79
$r_{0.1\%}$	35.9	6.68	5.10	27.36
$r_{0.01\%}$	78.5	7.95	11.22	59.13

Boltzmann method contains intrinsic and serious aeroacoustic capabilities and could achieve reliable results with few operations.

Table 3
Ratio for the number of operation between LBM and classical schemes for a dispersion error of 1%, 0.1% and 0.01%.

$R = \frac{N_{op}^{LBM}}{N_{op}^{NS}}$	Case 1	Case 2	Case 3
$R_{1\%}$	0.63	0.72	0.17
$R_{0.1\%}$	0.63	0.91	0.28
$R_{0.01\%}$	0.62	1.62	0.27

5. Conclusion

In this paper, we have studied the plane wave dispersion and dissipation for two kinds of discretization of the 3D linearized and isothermal Navier–Stokes equation: The lattice Boltzmann models and the high order schemes. A Von Neumann analysis of the isothermal and linearized Navier–Stokes equation has been made to reach the exact plane-wave solutions. The same analysis has been made on the discretized equations and the lattice Boltzmann models to get the dispersion and dissipation of the fully discrete Navier–Stokes equations and the different lattice Boltzmann schemes. The error terms of the lattice Boltzmann models and its influence on the dissipation has been clearly identified. The study of the LBM–BGK and the LBM–MRT models has highlighted the dispersion similarity of these models and the higher acoustic dissipation of the MRT model. However, the comparison between the different results has highlighted the low dissipative capabilities of the lattice Boltzmann models compared to the high order schemes. Even, if the lattice Boltzmann methods is of course more dispersive than the optimized high order schemes, it can be set between a second order scheme in space with a 3-step Runge–Kutta in time and an optimized third order with a 3-step Runge–Kutta algorithm. Finally, it has been shown that for a given dispersion error, the Lattice Boltzmann method was faster than the high order schemes. This study does not take into account stability problems. Low-dissipative schemes are often unstable and different solutions exists to damp the instabilities. We have seen for the LBM–MRT model that increasing the stability could lead to higher acoustic dissipation. The implementation of selective spatial filters in the lattice Boltzmann method will be part of our future work [25] and could lead to a better compromise between dissipation and stability.

Acknowledgements

This work has been done in the PREDIT project "MIMOSA", which receives a financial support from ADEME. We would like to thanks the reviewers of this paper for their relevant and constructive remarks.

Appendix

Here are the definition of the different matrices used in the paper.

(1) For the linearized Navier–Stokes equation:

$$\mathbf{M_E} = \begin{pmatrix} u_0 & 1 & 0 & 0 & 0 \\ 0 & u_0 - (\frac{4}{3}\nu + \xi)\frac{\partial}{\partial x} & (\frac{2}{3}\nu - \xi)\frac{\partial}{\partial y} & (\frac{2}{3}\nu - \xi)\frac{\partial}{\partial z} & 1 \\ 0 & -\nu\frac{\partial}{\partial y} & u_0 - \nu\frac{\partial}{\partial x} & 0 & 0 \\ 0 & -\nu\frac{\partial}{\partial z} & 0 & u_0 - \nu\frac{\partial}{\partial x} & 0 \\ 0 & c_0^2 & 0 & 0 & u_0 \end{pmatrix}$$

$$\mathbf{M_F} = \begin{pmatrix} v_0 & 0 & 1 & 0 & 0 \\ 0 & v_0 - \nu\frac{\partial}{\partial y} & -\nu\frac{\partial}{\partial x} & 0 & 0 \\ 0 & (\frac{2}{3}\nu - \xi)\frac{\partial}{\partial x} & v_0 - (\frac{4}{3}\nu + \xi)\frac{\partial}{\partial y} & (\frac{2}{3}\nu - \xi)\frac{\partial}{\partial z} & 1 \\ 0 & 0 & -\nu\frac{\partial}{\partial z} & v_0 - \nu\frac{\partial}{\partial y} & 0 \\ 0 & 0 & c_0^2 & 0 & v_0 \end{pmatrix}$$

$$\mathbf{M_G} = \begin{pmatrix} w_0 & 0 & 0 & 1 & 0 \\ 0 & w_0 - \nu\frac{\partial}{\partial z} & 0 & -\nu\frac{\partial}{\partial x} & 0 \\ 0 & 0 & w_0 - \nu\frac{\partial}{\partial z} & -\nu\frac{\partial}{\partial y} & 0 \\ 0 & (\frac{2}{3}\nu - \xi)\frac{\partial}{\partial x} & (\frac{2}{3}\nu - \xi)\frac{\partial}{\partial y} & w_0 - (\frac{4}{3}\nu + \xi)\frac{\partial}{\partial z} & 1 \\ 0 & 0 & 0 & c_0^2 & w_0 \end{pmatrix}$$

where c_0 is the sound speed defined by: $c_0^2 = \gamma\frac{p_0}{\rho_0}$.

$\mathbf{M}^{NS} = k_x\mathbf{M_E} + k_y\mathbf{M_F} + k_z\mathbf{M_G}$

(2) For the discretized linearized Navier–Stokes equations:

$$\mathbf{M}_d^{\mathrm{NS}} = \mathbf{I} + \sum_{j=1}^{p} \gamma_j (CFL)^j \mathbf{\Lambda}^j$$

$$\mathbf{\Lambda} = -\frac{\Delta x}{c_0}[Dx\mathbf{M}_{\mathbf{E}} + Dy\mathbf{M}_F + Dz\mathbf{M}_{\mathbf{G}}]$$

where Dx, Dy, Dz are the derivative operators given by Eq. (8).

(3) For the discrete velocities Boltzmann equation:

$$\mathbf{M}_{\alpha\beta}^{\mathrm{DVBE}} = \frac{1}{\tau}[\delta_{\alpha\beta} - \frac{\partial f_\alpha^{eq}}{\partial f_\beta}|_{f_\beta = f_\beta^{(0)}}] + i\mathbf{k}.\mathbf{c}_\alpha \delta_{\alpha\beta}$$

(4) For the lattice Boltzmann BGK equation:

$$\mathbf{M}^{\mathrm{BGK}} = A^{-1}\left[Id - \frac{1}{\tau_g} N^{\mathrm{BGK}}\right]$$

$$A_{\alpha\beta} = e^{i\mathbf{k}.\mathbf{c}_\alpha}\delta_{\alpha\beta}$$

$$N_{\alpha\beta}^{\mathrm{BGK}} = \delta_{\alpha\beta} - \frac{\partial g_\alpha^{eq}}{\partial g_\beta}|_{g_\beta = g_\beta^{(0)}}$$

(5) For the lattice Boltzmann MRT equation:

$$\mathbf{M}^{\mathrm{MRT}} = A^{-1}[Id - P^{-1}SN^{\mathrm{MRT}}P]$$

$$N_{\alpha\beta}^{\mathrm{MRT}} = \delta_{\alpha\beta} - \frac{\partial m_\alpha^{eq}}{\partial m_\beta}|_{m_\alpha = m_0}$$

The coefficients of P and S are given in [10]. Because the MRT model must recover the BGK model for $S = \frac{1}{\tau_g} I$, the equality of $\mathbf{M}^{\mathrm{MRT}}$ and $\mathbf{M}^{\mathrm{BGK}}$ leads to:

$$N^{\mathrm{MRT}} = PN^{\mathrm{BGK}}P^{-1} \tag{45}$$

References

[1] J. Berland, C. Bogey, C. Bailly, Low-dissipation and low-dispersion fourth order Runge–Kutta algorithm, Comput. Fluid 10 (2006) 35.
[2] P. Bhatnagar, E. Gross, M. Krook, A model for collision process in gases. I. Small amplitude process in charged and neutral one-component systems, Phys. Rev. 94 (3) (1954) 511–525.
[3] C. Bogey, C. Bailly, A family of low dissipative explicit schemes for flow and noise computations, J. Comput. Phys. 194 (2004) 194–214.
[4] J. Buick, C. Greated, D. Campbell, Lattice BGK simulation of sound waves, Europhys. Lett. 43 (3) (1998) 235–240.
[5] S. Chapman, T. Cowling, The Mathematical Theory of Non-Uniform Gases, third ed., Mathematical Library, Cambridge, 1991.
[6] H. Chen, W. Matthaeus, Recovery of Navier–Stokes equations using a lattice-gas Boltzmann method, Phys. Rev. A 45 (1992) R5339–R5342.
[7] S. Chen, G. Doolen, Lattice Boltzmann method for fluid flows, Annu. Rev. Fluid Mech. 161 (1998) 329.
[8] T. Colonius, S. Lele, Computational aeroacoustics: progress on nonlinear problems of sound generation, Prog. Aerospace Sci. 40 (2004) 345–416.
[9] P. Dellar, Bulk and shear viscosities in lattice Boltzmann equations, Phys. Rev. E 64 (2003).
[10] D. d'Humière, I. Ginzburg, Y. Krafczyk, P. Lallemand, L. Luo, Multiple relaxation time lattice Boltzmann models in three dimensions, Phil. Trans. Roy. Soc. Lond. A 360 (2002) 437–451.
[11] S. Geller, M. Krafczyk, J. Tölke, S. Turek, J. Hron, Benchmark computations based on lattice-Boltzmann, finite element and finite volume methods for laminar flows, Comput. Fluid 35 (2006) 888–897.
[12] J. Hardin, M. Hussaini, Computational Aeroacoustics: Presentations at the Workshop on CAA, ICASE/NASA LaRC, Springer-Verlag, New York, 1993.
[13] X. He, L. Luo, A priori derivation of the lattice Boltzmann equation, Phys. Rev. E 55 (1997) R6333.
[14] X. He, L. Luo, Lattice Boltzmann model for the incompressible Navier–Stokes equation, J. Stat. Phys. 88 (1997) 927–944.
[15] L. Kovasznay, Turbulence in supersonic flow, J. Aeronaut. Sci. 20 (1953) 657–682.
[16] P. Lallemand, L. Luo, Theory of the lattice Boltzmann method: dispersion, dissipation, isotropy, Galilean invariance and stability, Phys. Rev. E 61 (6) (2000).
[17] S. Lele, Compact finite difference schemes with spectral-like resolution, J. Comput. Phys. 103 (1) (1992) 16–42.
[18] R. Maier, R. Bernard, Accuracy of the lattice Boltzmann method, Int. J. Mod. Phys. C 84 (1997) 747–752.
[19] S. Marié, Etude de la mTthode Boltzmann sur RTseau pour les simulations en aTroacoustique, Ph.D. Thesis, UPMC, Univ Paris 06, 2008.
[20] S. Marié, D. Ricot, P. Sagaut, Accuracy of lattice Boltzmann method for aeroacoustics simulations, in: AIAA-Paper 2007-3515, 2007.
[21] Y.-H. Qian, D. d'Humières, P. Lallemand, Lattice BGK models for Navier–Stokes equation, Europhys. Lett. 17 (1992) 479–484.
[22] Y.-H. Qian, H. Zou, Complete Galilean-invariant lattice BGK models for the Navier–Stokes equation, Europhys. Lett. 42 (1998) 359.
[23] M. Reider, J. Sterling, Accuracy of discret-velocity BGK models for the simulation of the incompressible Navier–Stokes equation, Comput. Fluid 24 (1995) 459–467.
[24] D. Ricot, V. Maillard, C. Bailly, Numerical simulation of unsteady cavity flow using Lattice Boltzmann Method, in: AIAA-Paper 2002-2532, 2002.
[25] D. Ricot, S. Marié, P. Sagaut, C. Bailly, Lattice Boltzmann method with selective viscosity filter, J. Comput. Phys. (2008).
[26] P. Sagaut, C. Cambon, Homogeneous Turbulence Dynamics, Cambridge University Press, 2008.
[27] T. Sengupta, A. Dipankar, P. Sagaut, Error dynamics: beyond Von Neumann analysis, J. Comput. Phys. 226 (2) (2007) 1211–1218.
[28] J. Sterling, S. Chen, Stability analysis of lattice Boltzmann methods, J. Comput. Phys. 123 (1996) 196–206.
[29] C. Tam, Computational aeroacoustics: issues and methods, AIAA J. 10 (1995) 33.
[30] C. Tam, J. Webb, Dispersion relation preserving finite difference schemes for computational acoustics, J. Comput. Phys. 107 (1993) 262–281.
[31] A. Wilde, Application of the lattice Boltzmann method in flow acoustics, in: Fourth SWING Aeroacoustic Workshop, Aachen, 2004.